Optics Communications 549 (2023) 129891

Contents lists available at ScienceDirect

Optics Communications

journal homepage: www.elsevier.com/locate/optcom

Hybrid FSO/RF system over proposed random dust attenuation model based on real-time data combined with G–G atmospheric turbulence

Passant H. Mohamed *, Mohamed A. El-Shimy, Hossam M.H. Shalaby, Hassan Nadir Kheirallah

Electrical Engineering Department, Faculty of Engineering, Alexandria University, Alexandria 21544, Egypt

ARTICLE INFO

Keywords:
BPSK
Dust attenuation
FSO
Hybrid FSO/RF
Selection combining
Outage probability

ABSTRACT

Free-space optical (FSO) communication links are thought to be most negatively impacted by fog and sandstorms. Several probabilistic models for signal attenuation in various types of fog have been proposed in the literature. To the best of our knowledge, there is no prior probabilistic signal attenuation model for dusty channels. As a result, in this study, we analyse the probabilistic behaviour of the FSO channel during sandstorms using real-time data from the Egyptian Meteorological Authority and propose the negative-exponential (NE) distribution as a novel statistical model for signal attenuation in dust. A probability distribution function (PDF) is then derived for the random dust channel state. Also, a closed-form channel state distributional formulation is derived for a stochastic FSO channel model that considers both dust effects and Gamma–Gamma (G–G) atmospheric turbulence-induced fading. Next, closed formulas are derived for both the average bit-error rate (BER) and outage probability for the FSO system operating in this channel environment. Using the forms derived, it can be shown that the dust storm has a significant impact on the system's performance. Finally, to overcome this degradation, we suggest utilizing a hybrid FSO and radio frequency (RF) wireless communication system. The received signals are combined using the well-known diversity selection combining (SC) technique. Further, the hybrid system's performance was compared to that of an FSO-only system.

1. Introduction

One of the biggest issues in the 5G cellular network is the connection of its extremely dense traffic cells to the core network through fronthaul and backhaul transports [1]. Such a connection is mainly based on fibre optics for reliable transportation of high data rates. Free space optics (FSO) technology is now attracting a lot of interest as a fibre alternative since it transports data across free space, whereas building fibre optic connections can be expensive or even impossible in some regions [2]. In addition, FSO offers a number of benefits, such as rapid and simple installation, no licence fees, cost efficiency, a large bandwidth, and immunity to electromagnetic interference. However, adverse external weather conditions, including fog, dust, rain, and atmospheric turbulence, have a significant negative impact on FSO connectivity [3].

Apart from rain attenuation, the two main factors that can disrupt connections and limit visibility to a few metres are fog and sandstorms. This is because their particles' size is comparable to that of the light wavelength used in FSO systems. The majority of the FSO system research has been done in North America, East Asia, and Europe, where the most frequent weather patterns are turbulence, fog, rain, and snow [3]. To model various types of turbulence, there are numerous probabilistic models available, including G–G, Malaga, and K turbulence [4–7]. Furthermore, the authors in [8,9] proposed probabilistic models for continental moderate and dense fog. A novel probabilistic Gamma distribution was proposed by the author in [10] that fits various types of fog.

Regarding dust particles, there is a dearth of data and research on their impact on FSO due to their absence in the environment under investigation. Hence, their effect is frequently ignored. Dust storms happen in many other places around the world, such as the Middle East and North Africa, where we focus our studies. Any FSO connection installations in present and future communication networks in dry and semi-arid regions, will be extremely dependent on the dust effect.

Due to the unpredictability of dust storm episodes and the lack of knowledge regarding how they affect FSO links, some authors have built specialized experimental rooms to investigate the influence of sandstorms on the FSO channel [11–14]. The authors of [15,16] have

* Corresponding author.
E-mail addresses: passant.hosny@alexu.edu.eg (P.H. Mohamed), mohamed.elshimy@alexu.edu.eg (M.A. El-Shimy), shalaby@ieee.org (H.M.H. Shalaby), hassan.nadir@alexu.edu.eg (H.N. Kheirallah).

https://doi.org/10.1016/j.optcom.2023.129891
Received 12 January 2023; Received in revised form 10 May 2023; Accepted 1 September 2023
Available online 9 September 2023

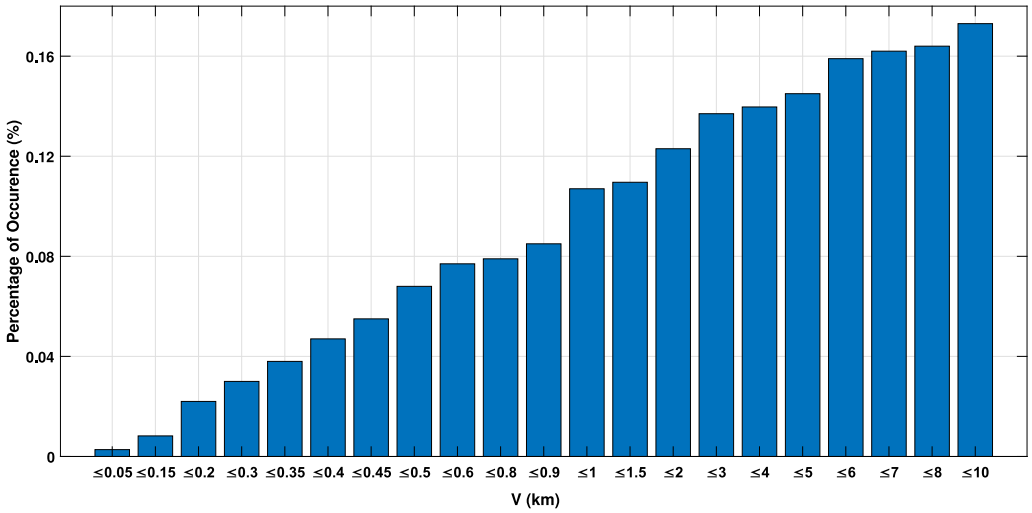

Fig. 1. Dust storm event for years 2018, 2019, and 2020 at El-Dabaa, Egypt.

also investigated experimentally the negative impact of dusty channels on the FSO link and attempted to improve the performance by employing a number of methods.

As far as we know, no prior probabilistic dust attenuation model exists. As a result, we concentrated our efforts on developing a probabilistic model based on real-time data to estimate attenuation caused by dust storms for the construction of the FSO connection and networking. Our study is based on measurements of reduced visibility brought on by sandstorms that were obtained from the Egyptian Meteorological Authority for the years 2018, 2019, and 2020 at the city of El-Dabaa, which is located on the north coast of Egypt, approximately 296 kilometres (184 miles) from Cairo. Since El-Dabaa's nature is comparable to that of any arid region, our proposed model can be used for any such environment.

The following are the key contributions of the paper:

- Based on measurements from the Egyptian Meteorological Authority, we suggest the negative-exponential (NE) distribution as a novel model for signal attenuation in dusty environments.
- We derive the probability density function (PDF) of the proposed dusty channel state.
- The PDF of the combined statistical effect of the proposed dust model with gamma–gamma (G–G) turbulence is also derived.
- We analyse the performance of the FSO system by developing novel closed-form expressions for the average bit-error rate (BER) of binary phase shift keying (BPSK) signals and outage probability in terms of the Meijer G-function.
- In order to identify which effect has a greater impact on the FSO system, the performance of the FSO system with dust attenuation and G–G turbulence is compared to the performance of the FSO system with dust attenuation only and G–G turbulence only in terms of the outage probability and the average BER.
- Using the derived novel closed formulas for both average BER and outage probability, we investigate a hybrid FSO/RF diversity selection combining (SC) method to improve the performance of FSO links as dust is often found to have negligible impact on the attenuation of microwave and millimetre wave (mmW) signals [15,17]. This approach does not require feedback information or additional channel state information (CSI) at the transceiver.
- A performance comparison study between hybrid and FSO-only link systems is then investigated according to the outage probability and the average BER.

The paper is organized as follows: Section 2 is devoted to a derivation for a signal attenuation probabilistic model in sandstorms. In Section 3, the FSO system model was studied and closed formulas for both average BER and outage probability were derived. The hybrid FSO/RF system model is presented in Section 4 along with a derivation for the corresponding average BER and outage probability. In Section 5, the obtained results are discussed and analysed. Finally, our conclusion is given in Section 6.

Table 1
Classification of dust events based on visibility ranges.

Dust type	Severe	Moderate	Light
V (km)	≤0.2	0.2–1	1–10

2. Dust attenuation modelling

In this section, we statistically examine the signal attenuation caused by dusty weather in an effort to identify a PDF that best fits this attenuation. In order to fulfil this purpose, a collection of real-time data on visibility owing to sandstorm events in the city of El-Dabaa, Egypt, for three consecutive years (2018, 2019, and 2020) was obtained from the Egyptian Meteorological Authority. The "visibility range" in kilometres (km) is the distance at which, under certain weather conditions, the picture contrast drops to 2% of what it would be if the item were nearby.

The graph in Fig. 1 depicts the random visibility data collected in the presence of sand storms. The obtained visibility ranges are divided into three types in accordance with the worldwide visibility code depicted in Table 1 to make our study of the system performance easier.

Our goal is to develop a probabilistic channel model for signal attenuation in the dusty environment that will allow us to estimate the influence of sand storms on FSO. The histograms in Figs. 2(a), 3(a), and 4(a) represent an approximate distribution of numerical data for severe, moderate, and light dust attenuation, respectively. The Freedman–Diaconis rule, as used in [18], was used to bin the range of data values on the x-axis. In statistics, the width of the bins is obtained from:

$$\text{Bin width} = 2 \times \frac{IQR(w)}{\sqrt[3]{r}}, \tag{1}$$

where $IQR(w)$ is the data's interquartile range and r is the number of observations in the w sample [19]. The PDF for the underlying variable is estimated from the histogram graph, which provides an approximate notion of the density of the underlying distribution of the data. Indeed,

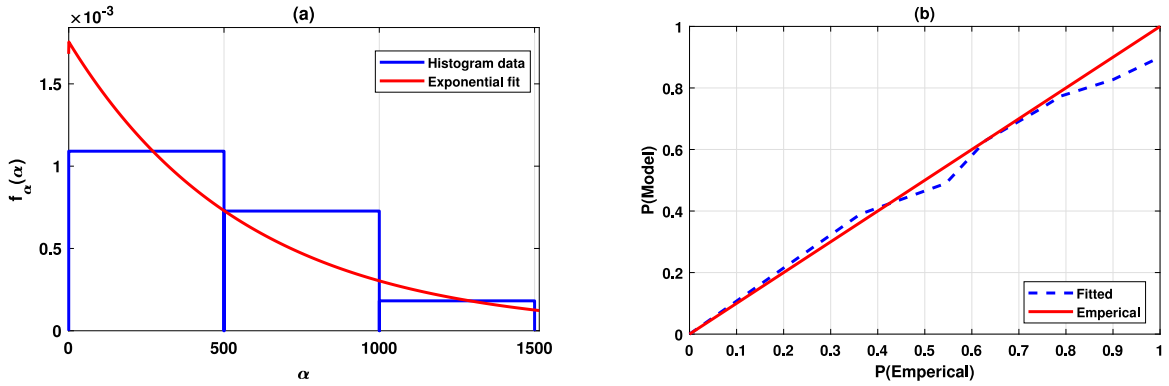

Fig. 2. Fitting severe dust attenuation to exponential distribution using MATLAB distribution fitter: (a) Moderate dust attenuation PDF. (b) Moderate dust attenuation probability plot.

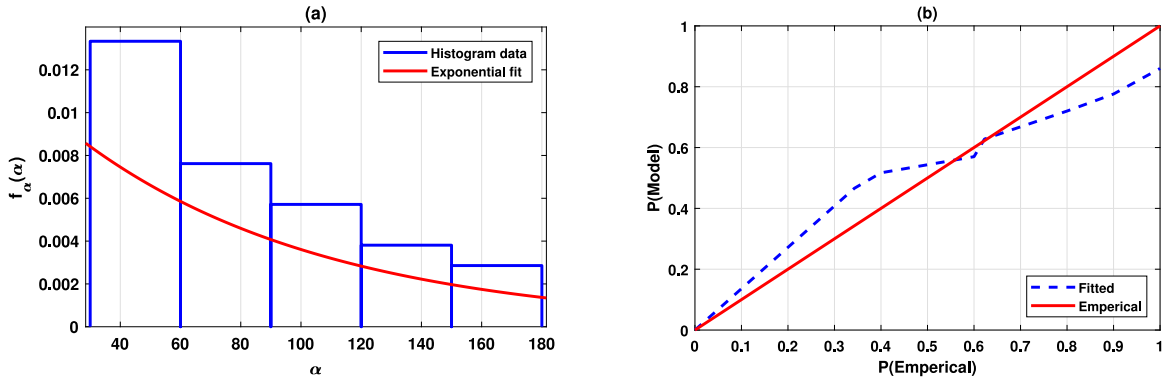

Fig. 3. Fitting moderate dust attenuation to exponential distribution using MATLAB distribution fitter: (a) Moderate dust attenuation PDF. (b) Moderate dust attenuation probability plot.

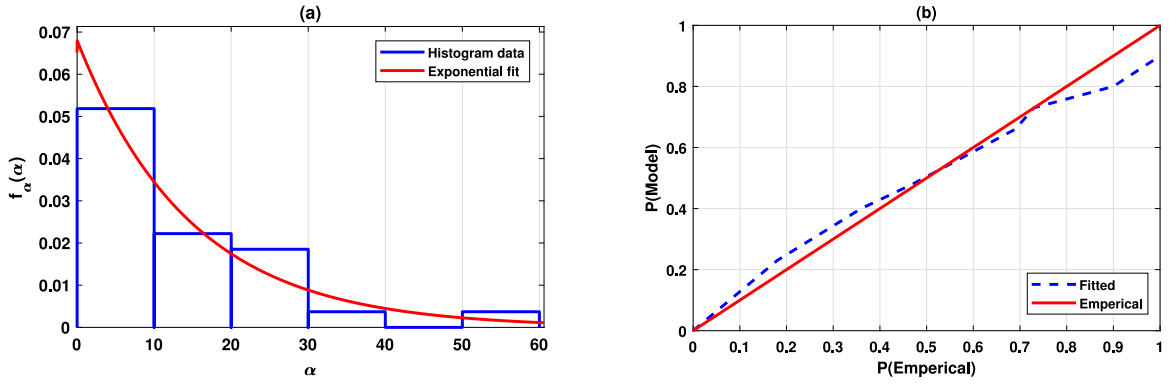

Fig. 4. Fitting light dust attenuation to exponential distribution using MATLAB distribution fitter: (a) light dust attenuation PDF. (b) light dust attenuation probability plot.

the frequency (probability) density is given by the number of values that fall within each interval (frequency) per unit.

We have investigated and compared various PDFs, including non-negative, limited, and unbounded continuous distributions, using the MATLAB distribution fitter application to fit the dust signal attenuation. Figs. 2, 3, and 4 show the empirical sample data versus NE fitting for the PDF and the probability plot (P–P) for severe, moderate, and light dust, respectively. We have identified that the NE distribution fits, with a high level of significance, the signal attenuation PDF. The NE distribution is given by:

$$f_{\alpha_l}(\alpha_l) = \frac{1}{\mu} \times e^{-\alpha_l/\mu} \tag{2}$$

where α_l (dB/km) is the signal attenuation due to dust and can be related to the visibility ranges obtained using [13] and $\mu > 0$ is the mean value of the NE distribution. Furthermore, the average value of μ was calculated for each dust visibility range (severe, moderate, and light), as shown in Table 2. It is clear that μ is directly proportional to dust density.

Table 2
Exponential mean value for various dust types.

Dust type	Severe	Moderate	Light
μ	550	100	15

The P–P plot compares fitted CDF values to empirical CDF values [20], and hence it is used to visually confirm the accuracy with which a given distribution fits a given set of measurements. The P–P plot will be approximately a diagonal line if the chosen CDF is the right

model. The P–P plots' approximately tight tracking of the diagonal line with occasional deviations demonstrate the exponential distribution's ability as a probabilistic model for signal attenuation in dust as shown in Figs. 2(b), 3(b), and 4(b).

3. System model

BPSK modulation is used in the FSO system under examination in this work. The additive white Gaussian noise (AWGN), proposed NE dust attenuation, and G–G atmospheric turbulence attenuate the signal during air travel; hence, direct detection results in an expression for the incoming signal in the form of:

$$y = h\mathcal{R}x + n_r \tag{3}$$

where h, $\mathcal{R}$, x, and n_r are the random channel state, detector responsivity, binary sent signal intensity, and AWGN, respectively. The random dust attenuation channel state (h_a) and the G–G atmospheric turbulence channel state (h_t) are combined to form the overall random channel state h as:

$$h = h_a \cdot h_t \tag{4}$$

Because FSO is a rapid communication network with data rates in gigabits per second, we assume the dusty channel is a slow-fading channel. In FSO channels, the symbol duration, measured in nanoseconds, is found to be much shorter than the channel coherence time, measured in milliseconds [3]. For a channel with gradual fading, the electrical signal-to-noise ratio (SNR) is represented by:

$$\gamma(h) = \overline{\gamma} \cdot h^2, \tag{5}$$

where the average SNR is given by $\overline{\gamma}$. The Beer–Lambert rule, which explains the relationship between signal attenuation and link length, characterizes the channel state under dusty conditions [21]:

$$h_a = \exp(-\alpha_k L), \tag{6}$$

where α_k is the attenuation coefficient in (km^{-1}) and L is the link length in (km). The signal attenuation α_l in (dB/km) is related to the attenuation coefficient as [22]:

$$\alpha_l = 4.343\ \alpha_k \tag{7}$$

From Eqs. (6) and (7), α_l in (dB/km) is related to h_a as:

$$\alpha_l = -\frac{4.343}{L} \ln h_a. \tag{8}$$

The signal attenuation PDF in dust, $f_{\alpha_l}(\alpha_l)$, can be used to determine the atmospheric channel state PDF as [23]:

$$f_{h_a}(h_a) = \sum_i f_{\alpha_l}(\alpha_l) \left| \frac{d\alpha_l}{dh_a} \right|_{\alpha_l=\alpha_{li}}, \tag{9}$$

where

$$\left| \frac{d\alpha_l}{dh_a} \right| = \frac{L \times h_a}{4.343}. \tag{10}$$

The index i in Eq. (9) represents the number of solutions for the variable α_l over the interval of interest ($0 \le h_a \le 1$). In our case, we have only one solution, represented by Eq. (8). Substituting Eqs. (2), (8), and (10) into Eq. (9) yields the PDF of the proposed dusty channel state $f_{h_a}(h_a)$:

$$f_{h_a}(h_a) = z \times h_a^{z-1}, \tag{11}$$

where $0 \le h_a \le 1$ and $z = \frac{4.343}{L\mu}$.

The PDF of the G–G turbulence channel state is given by [24]:

$$f_{h_t}(h_t) = \frac{2 \cdot (\alpha\beta)^{\frac{\alpha+\beta}{2}}}{\Gamma(\alpha) \cdot \Gamma(\beta)} \times h_t^{\frac{\alpha+\beta}{2}-1} \times K_{\alpha-\beta}(2\sqrt{\alpha\beta h_t}), \tag{12}$$

where $\Gamma(\cdot)$ is the gamma function, $K_x(\cdot)$ is the second type of modified Bessel function of order x. The effective number of large-scale cells in the scattering process is determined by α, whereas the quantity of fading is determined by β. Their values can be calculated as given in [24]. The previous PDFs for dust and G–G turbulence channel states, represented by Eqs. (11) and (12), are used to calculate the PDF of composite channel state h.

$$f_h(h) = \int f_{h|h_t}(h|h_t) f_{h_t}(h_t) dh_t, \tag{13}$$

where $f_{h|h_t}(h|h_t)$ is the conditional probability given h_t state and is expressed by:

$$f_{h|h_t}(h|h_t) = \frac{1}{h_t} \times f_{h_a}\left(\frac{h}{h_t}\right) = \frac{z}{h_t} \times \left(\frac{h}{h_t}\right)^{z-1}, \tag{14}$$

where $0 \le h \le h_t$. By substituting Eqs. (12) and (14) in Eq. (13), the composite channel state PDF is given by:

$$\begin{aligned} f_h(h) = \int_h^\infty \frac{z}{h_t} \times \left(\frac{h}{h_t}\right)^{z-1} \times \frac{2 \cdot (\alpha\beta)^{\frac{\alpha+\beta}{2}}}{\Gamma(\alpha) \cdot \Gamma(\beta)} \\ \times h_t^{\frac{\alpha+\beta}{2}-1} \times K_{\alpha-\beta}(2\sqrt{\alpha\beta h_t}) dh_t. \end{aligned} \tag{15}$$

In order to solve the integral in Eq. (15), we express the $K_v(.)$ in terms of the Meijer's G-function using [25]:

$$K_v(x) = \frac{1}{2} \cdot G_{0,2}^{2,0}\left(\frac{x^2}{4}\middle|_{\frac{v}{2},\frac{-v}{2}}\right). \tag{16}$$

Next using [26], a closed-form expression for the proposed composite channel state is derived as:

$$f_h(h) = \frac{z \cdot (\alpha\beta)^{\frac{\alpha+\beta}{2}}}{\Gamma(\alpha) \cdot \Gamma(\beta)} \times h^{\frac{\alpha+\beta}{2}-1} \times G_{1,3}^{3,0}\left(\alpha \cdot \beta \cdot h\middle|_{z-1,\alpha-1,\beta-1}^{z}\right). \tag{17}$$

3.1. FSO outage probability

The outage probability is the likelihood that the average SNR will drop below a specific threshold value, (γ_{th}). It is expressed as [27]:

$$P_{out} = P(\gamma \le \gamma_{th}). \tag{18}$$

3.1.1. Dust attenuation only

First, assuming only dust attenuation is affecting our system, an expression for the outage probability is driven as follows:

$$P_{out} = P(\overline{\gamma} \cdot h_a^2 \le \gamma_{th}) = P(h_a \le h_o), \tag{19}$$

where $h_o = \sqrt{\frac{\gamma_{th}}{\overline{\gamma}}}$. Hence, the probability of outage is the CDF of the channel state $F_\gamma(\gamma)$, where

$$P_{out} = F_\gamma(\gamma_{th}). \tag{20}$$

The outage probability P_{out} is given as:

$$P_{out} = \int_0^{h_0} f_{h_a}(h_a)\ \ dh_a. \tag{21}$$

Expressing h_a^z according to Meijer's G function using [26]:

$$h_a^z = G_{0,1}^{1,0}\left(h_a\middle|_z^-\right) + G_{1,2}^{1,1}\left(h_a\middle|_{z+1,z}^{z+1}\right) \tag{22}$$

Applying random variable transformation using [28], then solving this integral using [26], a closed form expression for the outage probability in case of dust attenuation only is obtained as:

$$\begin{aligned} P_{out} = \frac{z \cdot (2)^{z-3}}{\sqrt{\pi}} \times \left[G_{1,3}^{2,1}\left(\frac{\gamma_{th}}{16 \cdot \overline{\gamma}}\middle|_{\frac{z}{2},\frac{z+1}{2},0}^{1}\right) \right. \\ \left. + G_{1,3}^{1,2}\left(\frac{\gamma_{th}}{16 \cdot \overline{\gamma}}\middle|_{\frac{z}{2},\frac{z+1}{2},0}^{1}\right) \right]. \end{aligned} \tag{23}$$

3.1.2. G–G atmospheric turbulence only

The outage probability if only atmospheric turbulence is present is given as:

$$P_{out} = \int_0^{h_0} f_{h_t}(h_t)\ \ dh_t. \tag{24}$$

Applying random variable transformation using [28], and solving this integral using [26], a closed form expression is given as:

$$P_{out} = \frac{(2)^{\alpha+\beta-2}}{\pi \cdot \Gamma(\alpha) \cdot \Gamma(\beta)} \times G_{1,5}^{4,1}\left(\frac{(\alpha\beta)^2 \cdot \gamma_{th}}{16 \cdot \overline{\gamma}}\middle|_{\frac{\alpha}{2}, \frac{\alpha+1}{2}, \frac{\beta}{2}, \frac{\beta+1}{2}, 0}^{1}\right). \tag{25}$$

3.1.3. Dust attenuation combined with G–G turbulence

The outage probability when both dust attenuation and G–G turbulence are effecting the FSO link, P_{out}, is given as:

$$P_{out} = \int_0^{h_0} \frac{z}{\Gamma(\alpha) \cdot \Gamma(\beta)} \times h^{-1} \times G_{1,3}^{3,0}\left(\alpha \cdot \beta \cdot h\middle|_{z,\alpha,\beta}^{z+1}\right) dh. \tag{26}$$

Using Eq. (5), $h = \sqrt{\frac{\gamma}{\overline{\gamma}}}$, utilizing [28], Eq. (26) can be written as:

$$P_{out} = \int_0^{\gamma_{th}} \frac{z}{2 \cdot \Gamma(\alpha) \cdot \Gamma(\beta)} \times \gamma^{-1} \times G_{1,3}^{3,0}\left(\frac{\alpha \cdot \beta}{\sqrt{\overline{\gamma}}} \sqrt{\gamma}\middle|_{z,\alpha,\beta}^{z+1}\right) d\gamma. \tag{27}$$

Using [26] a closed form for the proposed model outage probability is:

$$P_{out} = \frac{z \cdot (2)^{\alpha+\beta-3}}{\pi \cdot \Gamma(\alpha) \cdot \Gamma(\beta)} \times G_{3,7}^{6,1}\left(\frac{(\alpha\beta)^2 \cdot \gamma_{th}}{16 \cdot \overline{\gamma}}\middle|_{\frac{z}{2}, \frac{z+1}{2}, \frac{\alpha}{2}, \frac{\alpha+1}{2}, \frac{\beta}{2}, \frac{\beta+1}{2}, 0}^{1, \frac{z+1}{2}, \frac{z+2}{2}}\right). \tag{28}$$

3.2. FSO average BER

The average BER is one of the performance indicators that most accurately describes the nature of system behaviour. The BER of BPSK conditioned on h is given as [29]:

$$P_b(e|h) = \frac{1}{2} \times \mathrm{erfc}(\sqrt{\gamma}), \tag{29}$$

where $\mathrm{erfc}(\cdot)$ is the complementary error function.

3.2.1. Dust attenuation only

By averaging Eq. (26) over the PDF of h_a, it is possible to determine the average BER, $Pb(e)$, when only dust attenuation is taken into consideration:

$$P_b(e) = \int_0^{\infty} f_{h_a}(h_a) P_b(e|h_a)\ \ dh_a, \tag{30}$$

Then, expressing h_a^z according to Meijer's G function as Eq. (22). A closed form expression for the BER is obtained using [26]:

$$P_b(e) = \frac{z \cdot (2)^{z-1}}{\pi} \times \left[G_{3,2}^{2,2}\left(4 \cdot \overline{\gamma}\middle|_{0, \frac{1}{2}}^{1, \frac{1-z}{2}, \frac{2-z}{2}}\right) + G_{4,3}^{4,1}\left(4 \cdot \overline{\gamma}\middle|_{0, \frac{1}{2}, \frac{-z}{2}}^{1, \frac{-z}{2}, \frac{1-z}{2}, \frac{2-z}{2}}\right) \right] \tag{31}$$

3.2.2. Atmospheric turbulence only

In order to obtain a closed form for the BER in case of G–G turbulence only Eq. (26) is averaged over the PDF of h_t as:

$$P_b(e) = \int_0^{\infty} f_{h_t}(h_t) P_b(e|h_t)\ \ dh_t, \tag{32}$$

A closed form expression for the BER is obtained using [26]:

$$P_b(e) = \frac{(2)^{\alpha+\beta-3}}{\pi^{\frac{3}{2}} \cdot \Gamma(\alpha) \cdot \Gamma(\beta)} \times G_{5,2}^{2,4}\left(\frac{16 \cdot \overline{\gamma}}{(\alpha\beta)^2}\middle|_{0, \frac{1}{2}}^{\frac{1-\alpha}{2}, \frac{2-\alpha}{2}, \frac{1-\beta}{2}, \frac{2-\beta}{2}, 1}\right). \tag{33}$$

3.2.3. Dust attenuation combined with G-G turbulence

By averaging Eq. (26) over the PDF of h given in Eq. (17), it is possible to determine the average BER, $Pb(e)$:

$$P_b(e) = \int_0^{\infty} f_h(h) P_b(e|h)\ \ dh, \tag{34}$$

Then, substituting Eqs. (17) and (26) in Eq. (27), and expressing $\mathrm{erfc}(\cdot)$ in terms of Meijer's G-functions using [26], i.e., $\mathrm{erfc}(\sqrt{x}) = \frac{1}{\sqrt{\pi}} \cdot G_{1,2}^{2,0}\left(x\middle|_{o, \frac{1}{2}}^{1}\right)$. A closed-form solution for average BER of the proposed model is derived as:

$$P_b(e) = \frac{z \cdot (2)^{\alpha+\beta-4}}{\pi^{\frac{3}{2}} \cdot \Gamma(\alpha) \cdot \Gamma(\beta)} \times G_{6,3}^{2,5}\left(\frac{2 \cdot \overline{\gamma}}{(\alpha\beta)^2}\middle|_{0, \frac{1}{2}, \frac{-z}{2}}^{\frac{2-z}{2}, \frac{1-\alpha}{2}, \frac{1-\beta}{2}, \frac{1-\beta}{2}, \frac{2-\beta}{2}, 1}\right). \tag{35}$$

4. Hybrid FSO/RF system

Dust attenuation has a negative impact on the BER and outage probability of the FSO channel. However, the dust incidence has no significant impact on the RF system [15,17]. Combining the FSO link with a mmW RF link, which may achieve data rates comparable to the FSO link, is one means of increasing the FSO link's dependability and efficiency. Implementations of hybrid RF/FSO systems often fall into one of two categories: simultaneous transmission systems or switchover systems.

In the literature, various ways to switching between the RF and FSO links have been discussed. Authors in [30] presented a hard switching technique in which only the FSO connection operates until its SNR falls below a particular threshold, at which point the data is switched to be transmitted only over the RF link. The fundamental disadvantage of this approach is that it requires frequent hardware switching between the FSO and RF lines. Soft switching, an improved switching mechanism, was presented in [31]. Hybrid switching was proposed in [32], where the FSO connection is used primarily for data transfer as long as its quality (in terms of SNR) exceeds a threshold and the RF link is turned off. When the FSO link breaks, the system activates the RF link, and both lines communicate the same data at the same data rate. The receiver uses maximal ratio combining (MRC) to retrieve the original data. When the FSO link quality is satisfactory, the RF link is returned to standby mode.

Overall, depending on the operational subsystem, data in different switching systems can be provided at different data rates. For example, if the FSO subsystem SNR is greater than a given threshold value, data is sent at the FSO high data rate. When the FSO SNR goes below a specific threshold, the data rate is restricted to the RF link. In all switchover systems, the transmitter requires feedback information or instantaneous CSI for the switching operation, which frequently results in data rate loss [24]. Furthermore, the practical implementation of this type of scheme is both costly and complex [30].

Conversely, with simultaneous transmission hybrid systems, identical data with same data rate is transferred concurrently over both connections without experiencing over-switching issues. To handle the transmitting information before demodulation, this type of hybrid FSO/RF system requires diversity combining at the receiver [24,33]. As a result, there is no need for feedback information or additional CSI for the switching operation between the two connections, resulting

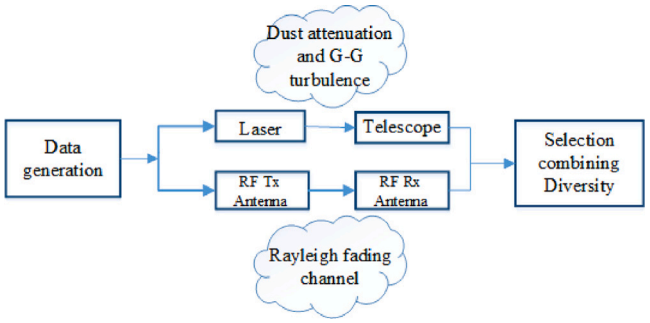

Fig. 5. Adopted hybrid FSO/RF system.

in a relatively simple and inexpensive architecture in comparison to switchover systems. The application of diversity combining techniques and their impact on hybrid FSO/RF systems are investigated in [34].

An FSO sub-system is integrated with a 60 GHz mmW subsystem that can provide data rates comparable to the FSO connection in our hybrid FSO/RF system, as demonstrated in Fig. 5. Data is delivered to both subsystems at the same time and at the same data rate, and then the receiver selection combining (SC) diversity technique is employed to select the connection with the highest SNR.

4.1. FSO subsystem

Under the assumption that 60 GHz mmW and FSO subsystems support the same data rates, the information stream is modulated using the BPSK digital scheme at the transmitter. The FSO sub-system under consideration is influenced by the proposed dust attenuation combined with G–G atmospheric turbulence.

From Eq. (20), it is clear that the CDF of the FSO subsystem can be obtained from the outage probability in Eq. (28) by replacing γ_{th} and γ_1, hence the CDF of the FSO subsystem is given as:

$$F_{\gamma_1}(\gamma_1) = \frac{z\cdot(2)^{\alpha+\beta-3}}{\pi\cdot\Gamma(\alpha)\cdot\Gamma(\beta)} \times G_{3,7}^{6,1}\left(\frac{(\alpha\beta)^2\cdot\gamma_1}{16\cdot\overline{\gamma_1}}\middle|_{\frac{z}{2},\frac{z+1}{2},\frac{\alpha}{2},\frac{\alpha+1}{2},\frac{\beta}{2},\frac{\beta+1}{2},0}^{1,\frac{z+1}{2},\frac{z+2}{2}}\right), \tag{36}$$

where γ_1 is the instantaneous electrical SNR at the receiver of the FSO sub-system and $\overline{\gamma_1}$ is the average electrical SNR.

4.2. RF subsystem

The BPSK-modulated signal x is up-converted to a mmW RF carrier frequency of 60 GHz at the RF sub-system's transmitter before being transmitted via the RF link. The RF signal is down-converted and demodulated at the RF sub-system receiver to recover the original data. Dust attenuation and atmospheric turbulence have no significant impact on the RF link; hence, they are not taken into consideration [17, 24]. As an alternative, we assume that the RF link has a Rayleigh fading channel.

The RF received signal y_{RF} is expressed by [35]:

$$y_{RF} = h_{RF}x + n_r, \tag{37}$$

where h_{RF} is the Rayleigh fading channel, x is the BPSK transmitted signal, and n_r is the AWGN. The RF subsystem's receiver's SNR is stated as [35]:

$$\gamma_2 = \frac{P_{RF}\times h_{RF}^2}{N_o}, \tag{38}$$

where P_{RF} is the signal's power as it travels across the RF channel and N_o is the noise power spectral density.

As a function of the link's SNR γ_2, the Rayleigh fading channel's PDF is denoted by the symbol $f_{\gamma_2}(\gamma_2)$ and is expressed as [35]:

$$f_{\gamma_2}(\gamma_2) = \frac{1}{\overline{\gamma_2}} \times \exp\left(-\frac{\gamma_2}{\overline{\gamma_2}}\right), \tag{39}$$

where $\overline{\gamma_2}$ is the average SNR of the RF fading channel. According to the SNR of the RF link's γ_2, the CDF of the Rayleigh channel $F_{\gamma_2}(\gamma_2)$ is provided by the formula [35]:

$$F_{\gamma_2}(\gamma_2) = 1 - \exp\left(-\frac{\gamma_2}{\overline{\gamma_2}}\right). \tag{40}$$

4.3. Hybrid FSO/RF system SC scheme

The diversity SC scheme is a representation of the most fundamental and straightforward combining technique. The SC evaluates the electrical SNR of each link and selects the signal with the greatest electrical SNR. As a result, the SNR (γ_{sc}) of the selection combiner is given as [34]:

$$\gamma_{sc} = \max(\gamma_1, \gamma_2). \tag{41}$$

The CDF of the selection combiner SNR $F_{\gamma_{sc}}(\gamma_{sc})$ follows as a result [34]:

$$F_{\gamma_{sc}}(\gamma_{sc}) = F_{\gamma_1}(\gamma_1)\cdot F_{\gamma_2}(\gamma_2). \tag{42}$$

Finally, by substituting Eqs. (36) and (40) in Eq. (42), the CDF of γ_{sc} is obtained as:

$$F_{\gamma_{sc}}(\gamma_{sc}) = \frac{z\cdot(2)^{\alpha+\beta-3}}{\pi\cdot\Gamma(\alpha)\cdot\Gamma(\beta)} \times \left(1-\exp(\frac{-\gamma_{sc}}{\overline{\gamma_{sc}}})\right) \times G_{3,7}^{6,1}\left(\frac{(\alpha\beta)^2\cdot\gamma_{sc}}{16\cdot\overline{\gamma_{sc}}}\middle|_{\frac{z}{2},\frac{z+1}{2},\frac{\alpha}{2},\frac{\alpha+1}{2},\frac{\beta}{2},\frac{\beta+1}{2},0}^{1,\frac{z+1}{2},\frac{z+2}{2}}\right). \tag{43}$$

4.3.1. FSO/RF SC outage probability

By substituting the SNR value in the link's CDF equation with the SNR threshold value γ_{th}, the outage probability of the hybrid FSO/RF system P_{out} is obtained.

$$P_{out} = \frac{z\cdot(2)^{\alpha+\beta-3}}{\pi\cdot\Gamma(\alpha)\cdot\Gamma(\beta)} \times \left(1-\exp(\frac{-\gamma_{th}}{\overline{\gamma_{sc}}})\right) \times G_{3,7}^{6,1}\left(\frac{(\alpha\beta)^2\cdot\gamma_{th}}{16\cdot\overline{\gamma_{sc}}}\middle|_{\frac{z}{2},\frac{z+1}{2},\frac{\alpha}{2},\frac{\alpha+1}{2},\frac{\beta}{2},\frac{\beta+1}{2},0}^{1,\frac{z+1}{2},\frac{z+2}{2}}\right). \tag{44}$$

4.3.2. FSO/RF SC average BER

In terms of the hybrid system SNR γ_{sc}, a novel closed-form formulation for the average BER $P_b(e)$ of the hybrid FSO/RF system is developed. The following is how this method applies the dual-branch SC receiver's BER expression [36]:

$$P_b(e) = \int_0^\infty e^{-q\gamma_{sc}}\ \gamma_{sc}^{p-1} F_{sc}(\gamma_{sc})\ d\gamma_{sc}, \tag{45}$$

where, $p = 1/2$, $q = 1$, when $M = 2$ (BPSK), and $p = 2/\log_2(M)$,

$q = \sin^2(\pi/M)$, when $M > 2$. By substituting Eq. (43) in Eq. (45)), and using [26], the average BER closed-form expression is obtained as in Eq. (46). Here $k = \frac{z\times 2^{\alpha+\beta-4}}{\pi\Gamma(p)\Gamma(\alpha)\Gamma(\beta)}$.

$$P_b(e) = k\cdot G_{4,7}^{6,2}\left(\frac{(\alpha\beta)^2}{16\cdot q\cdot\overline{\gamma}}\middle|_{\frac{z}{2},\frac{z+1}{2},\frac{\alpha}{2},\frac{\alpha+1}{2},\frac{\beta}{2},\frac{\beta+1}{2},0}^{1-p,1,\frac{z+1}{2},\frac{z+2}{2}}\right) - k\cdot(\frac{1}{\overline{\gamma}}+q)^{-p} \times G_{4,7}^{6,2}\left(\frac{(\alpha\beta)^2}{16\cdot(1+q\cdot\overline{\gamma})}\middle|_{\frac{z}{2},\frac{z+1}{2},\frac{\alpha}{2},\frac{\alpha+1}{2},\frac{\beta}{2},\frac{\beta+1}{2},0}^{1-p,1,\frac{z+1}{2},\frac{z+2}{2}}\right). \tag{46}$$

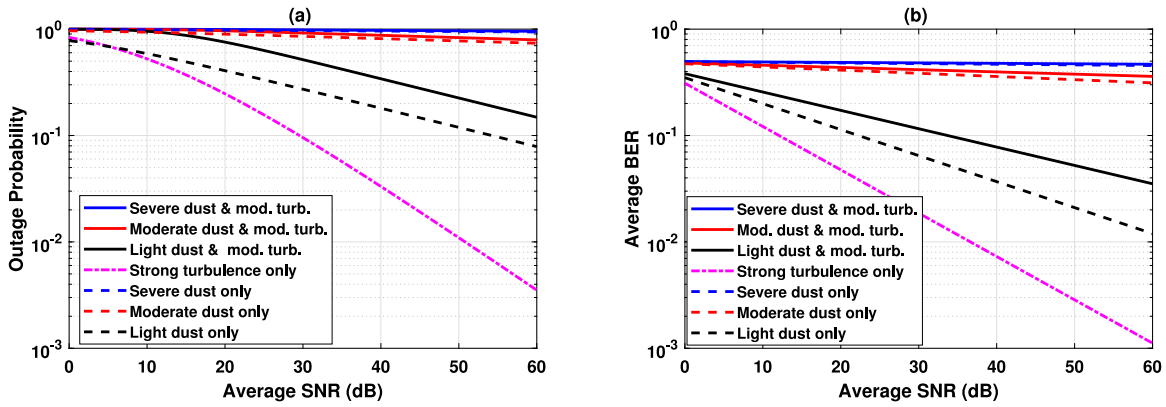

Fig. 6. (a) Outage probability vs. average SNR over FSO system at $L = 1$ km, and (b) Average BER vs. average SNR over FSO system at $L = 1$ km.

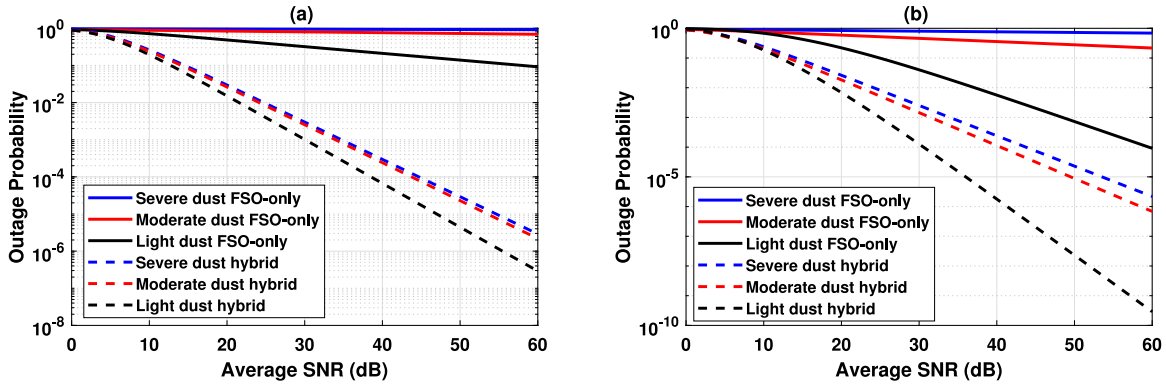

Fig. 7. Outage probability versus average SNR over FSO-only and hybrid FSO/RF channels with moderate turbulence: (a) $L = 1$ km, and (b) $L = 0.2$ km.

5. Results and discussion

In this section, it is first determined which phenomenon is more significant by comparing the performance of the FSO system affected by dust attenuation combined with G–G turbulence to that of dust attenuation alone and G–G turbulence alone. Under various dust circumstances, the average BER and outage probability are studied and compared for the three different scenarios using the resulting closed formulas obtained in Section 3.

Then, the performance of the hybrid FSO/RF system investigated in Section 4 is compared to that of the FSO-only system influenced by dust attenuation combined with moderate turbulence. The average BER and outage probability are investigated using the derived closed formulae over various dust conditions.

Two potential transmission link lengths of 1 km and 0.2 km are taken into consideration in our analysis. Our results could have applications in wireless communication systems of the future 5G generation, where these selected lengths might be similar to inter-base station distances, where the length of these cells might range from a few tens of metres to many hundreds (see Figs. 6–8). .

5.1. Outage probability

In Fig. 6(a), the outage probability of the FSO system is plotted vs. the average SNR at $L = 1$ km, it can be shown from the results that the FSO system under severe dust only has approximately the same outage probability of 0.9408 at 60 dB average SNR as the link influenced by severe dust combined with moderate G–G turbulence. However, for the case of moderate dust storms at 60 dB average SNR the FSO link effected by only moderate dust storms has an outage probability of 0.7407 while the link influenced by moderate dust combined with moderate turbulence has an 0.7922 outage probability at the same average SNR. The results reveal that the effects of severe and moderate dust storms are more dominant and have a greater impact on the FSO link in comparison to the influence of turbulence, which can be ignored in these conditions.

For light dust condition, the FSO link affected by dust only has an outage probability of 0.08199 at 60 dB average SNR; however, the outage probability of the FSO link influenced by light dust and moderate turbulence increased to 0.1485 at the same average SNR. When the effect of strong turbulence which produced an outage probability of 0.003519 at 60 dB average SNR—is compared to that of light dust paired with G–G moderate turbulence it is evident that the influence of strong turbulence is even better.

The outage probability of the FSO-only system is compared to that of the hybrid FSO/RF system in Figs. 7(a) and 7(b) for link lengths of 1 and 0.2 km, respectively. The outage probability is plotted versus the average electrical SNR ($\overline{\gamma}$), while a threshold SNR (γ_{th}) of 6 dB is assumed. Overall, the results indicate that no matter the link length, the FSO system performs very poorly under both severe and moderate dust. For an FSO 1 km link, the probability of an outage at a 40 dB SNR is 0.9343 and 0.7626 under severe and moderate dust, respectively. On the shorter link, the outage probability decreased to 0.7626 and 0.3577 for severe and moderate dust, respectively, at the same SNR value. However, for the hybrid FSO/RF system, the outage probability is enhanced to 10^{-3} for both link lengths under all dust types with an SNR value less than 35 dB.

The outage probability for the longer link under light dust is 0.2116, which is enhanced by the hybrid system to 10^{-3} at 30 dB SNR. However, for the 0.2 km FSO link, it achieved an outage probability

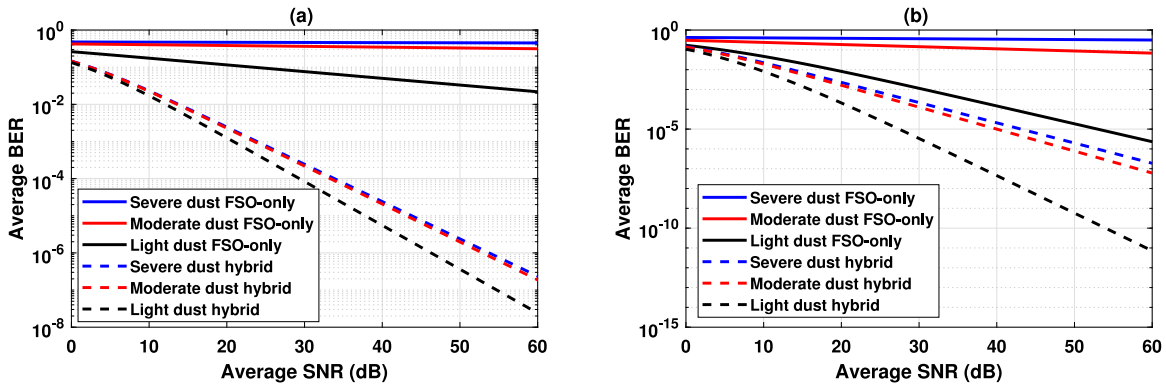

Fig. 8. Average BER versus average SNR over FSO-only and hybrid FSO/RF channels with moderate turbulence: (a) $L = 1$ km, and (b) $L = 0.2$ km.

of 10^{-3} at an SNR value of 48 dB; it also achieved the same outage probability at an SNR of 24 dB when using the hybrid system.

5.2. Average BER

In Fig. 6(b), the average BER of the FSO system is plotted vs. the average SNR at $L = 1$ km, the results depict that the effect of turbulence could be negligible in case of severe dust storms, as the BER of severe dust alone and the BER of severe dust combined with moderate turbulence are approximately equal and gave a BER of 0.4549 at 60 dB average SNR. Also, for the case of moderate dust, there was no significant effect of the turbulence on the link; the moderate dust only has a BER of 0.3125, while moderate dust combined with moderate turbulence has a BER of 0.3596 under the same average SNR.

The BER of the FSO system under light dust storms only affecting the system is 0.01196 at 60 dB average SNR, while in the case of moderate turbulence combined with light dust, a BER of 0.03591 is achieved at the same average SNR. It is clear that under light dust, the effect of turbulence must be taken into consideration and cannot be neglected. The case of strong turbulence only has a BER of 0.001117 at 60 dB average SNR, which gives a better performance than light dust alone or light dust combined with moderate turbulence; hence, we could conclude the major effect of dust storms on the FSO link.

In Figs. 8(a), and 8(b), the average BER is plotted versus the average electrical SNR $\bar{\gamma}$ to compare the performance of both the FSO-only and the hybrid FSO/RF systems for two different transmission lengths of 1 and 0.2 km over various dust conditions. The results show that the BER values significantly decrease with increasing dust density. Thus, for links with lengths of 1 km and 0.2 km, respectively, the average BER values are 0.4581 and 0.3462 under conditions of severe dust. Additionally, it can be seen that performance for moderate dust is better than for severe dust, but it still has high BER values of 0.3462 and 0.1126 for connection lengths of 1 km and 0.2 km, respectively.

The results show that even with a short connection length of 0.2 km, the system performance is very bad under both severe and moderate dust, with a very high BER. However, when using the proposed hybrid FSO/RF SC for the 1 km link, the BER drops to 10^{-3} at SNRs of 24.31 dB and 23.45 dB, respectively, under dense and moderate dust. Additionally, to achieve a BER of 10^{-3} for the 0.2 km link, the system required SNR values of 20.71 dB, and 19.64 dB under severe and moderate dust, respectively. The hybrid FSO/RF system is clearly superior in the case of severe and moderate dust, even for the 1 km link, as it can achieve a BER of 10^{-3} at an acceptable SNR value.

The system achieves an acceptable BER value of 10^{-3} at 30 dB SNR for the 0.2 km FSO-only link under light dust conditions. However, for the 1 km link with an average SNR 40 dB, the BER value is 0.05012 under light dust condition. As a result, we can conclude that a hybrid FSO/RF is a good solution for a 1 km link in light dust, with a 10^{-3} BER at 20.47 dB SNR. Although, for a 0.2 km FSO-only link, an acceptable BER can be achieved under light dust.

6. Conclusion

Due to the fact that most research has been carried out in locations devoid of a dusty environment, the majority of literature has ignored the impact of dust storms on FSO communication links. In this study, we have investigated the impact of dust storms using a proposed probabilistic dust attenuation model following the NE distribution that has been put forth to forecast system performance. Our results indicate that dust storms have significant influences on system performance, so maintaining a reliable communication link under severe and moderate dust is impossible regardless of the link length. However, the FSO link can perform under light dust with a short link length of 0.2 km. As a result, a hybrid FSO/RF SC diversity scheme has been adopted in this environment. Our results showed that, at all dust densities, the adopted system successfully improved the performance by utilizing the complementary features of FSO and RF channels.

Declaration of competing interest

The authors declare that they have no known competing financial interests or personal relationships that could have appeared to influence the work reported in this paper.

Data availability

Data will be made available on request.

References

[1] X. Ge, S. Tu, G. Mao, C.-X. Wang, T. Han, 5G ultra-dense cellular networks, IEEE Wirel. Commun. 23 (1) (2016) 72–79.
[2] M. Alzenad, M.Z. Shakir, H. Yanikomeroglu, M.-S. Alouini, FSO-based vertical backhaul/fronthaul framework for 5G+ wireless networks, IEEE Commun. Mag. 56 (1) (2018) 218–224.
[3] M.A. Khalighi, M. Uysal, Survey on free space optical communication: A communication theory perspective, IEEE Commun. Surv. Tutor. 16 (4) (2014) 2231–2258.
[4] A.G. AbdElKader, A. Allam, K. Kato, H.M. Shalaby, Performance enhancement of MRR underwater optical communications using LQAM-MPPM, in: 2022 Asia Communications and Photonics Conference, ACP, IEEE, 2022, pp. 473–476.
[5] A.E.-R.A. El-Fikky, A.S. Ghazy, H.S. Khallaf, E.M. Mohamed, H.M. Shalaby, M.H. Aly, On the performance of adaptive hybrid MQAM–MPPM scheme over Nakagami and log-normal dynamic visible light communication channels, Appl. Opt. 59 (7) (2020) 1896–1906.
[6] G.D. Roumelas, H.E. Nistazakis, E. Leitgeb, H.D. Ivanov, C. Volos, G.S. Tombras, Serially DF relayed hybrid FSO/MMW links with Weibull fading, M-turbulence and pointing errors, Optik 216 (2020) 164531.
[7] H.G. Sandalidis, T.A. Tsiftsis, G.K. Karagiannidis, M. Uysal, BER performance of FSO links over strong atmospheric turbulence channels with pointing errors, IEEE Commun. Lett. 12 (1) (2008) 44–46, http://dx.doi.org/10.1109/LCOMM.2008.071408.
[8] M.S. Awan, E. Leitgeb, C. Capsoni, R. Nebuloni, F. Nadeem, M.S. Khan, et al., Attenuation analysis for optical wireless link measurements under moderate continental fog conditions at Milan and Graz, in: 2008 IEEE 68th Vehicular Technology Conference, IEEE, 2008, pp. 1–5.

[9] F. Nadeem, T. Javornik, E. Leitgeb, V. Kvicera, G. Kandus, Continental fog attenuation empirical relationship from measured visibility data, Radioengineering 19 (4) (2010) 596–600.
[10] M.A. Esmail, H. Fathallah, M.-S. Alouini, On the performance of optical wireless links over random foggy channels, IEEE Access 5 (2017) 2894–2903.
[11] K. Su, L. Moeller, R.B. Barat, J.F. Federici, Experimental comparison of terahertz and infrared data signal attenuation in dust clouds, J. Opt. Soc. Amer. A 29 (11) (2012) 2360–2366.
[12] Z. Ghassemlooy, J. Perez, E. Leitgeb, On the performance of FSO communications links under sandstorm conditions, in: Proceedings of the 12th International Conference on Telecommunications, IEEE, 2013, pp. 53–58.
[13] M.A. Esmail, H. Fathallah, M.-S. Alouini, An experimental study of FSO link performance in desert environment, IEEE Commun. Lett. 20 (9) (2016) 1888–1891.
[14] H. Zhong, J. Zhou, Z. Du, L. Xie, A laboratory experimental study on laser attenuations by dust/sand storms, J. Aerosol Sci. 121 (2018) 31–37.
[15] M.A. Esmail, A.M. Ragheb, H.A. Fathallah, M. Altamimi, S.A. Alshebeili, 5G-28 GHz signal transmission over hybrid all-optical FSO/RF link in dusty weather conditions, IEEE Access 7 (2019) 24404–24410.
[16] M. Singh, S.N. Pottoo, J. Malhotra, A. Grover, M.H. Aly, Millimeter-wave hybrid OFDM-MDM radio over free space optical transceiver for 5G services in desert environment, Alex. Eng. J. 60 (5) (2021) 4275–4285.
[17] A. Musa, S.O. Bashir, A.H. Abdalla, Review and assessment of electromagnetic wave propagation in sand and dust storms at microwave and millimeter wave bands—Part I, Progr. Electromagnet. Res. M 40 (2014) 91–100.
[18] D. Freedman, P. Diaconis, On the histogram as a density estimator: L 2 theory, Z. Wahrscheinlichkeitstheor. verwandte Geb. 57 (4) (1981) 453–476.
[19] F.M. Dekking, C. Kraaikamp, H.P. Lopuhaä, L.E. Meester, A Modern Introduction to Probability and Statistics: Understanding Why and How, Vol. 488, Springer, 2005.
[20] J.D. Jobson, Applied Multivariate Data Analysis: Regression and Experimental Design, Springer Science & Business Media, 2012.
[21] A.A. Farid, S. Hranilovic, Outage capacity optimization for free-space optical links with pointing errors, J. Lightw. Technol. 25 (7) (2007) 1702–1710.
[22] G. Keiser, FTTX Concepts and Applications, John Wiley and Sons, 2006.
[23] A. Leon-Garcia, Probability and Random Processes for Electrical Engineering, Pearson Education India, 1994.
[24] W.M.R. Shakir, Performance evaluation of a selection combining scheme for the hybrid FSO/RF system, IEEE Photonics J. 10 (1) (2017) 1–10.
[25] V. Adamchik, O. Marichev, The algorithm for calculating integrals of hypergeometric type functions and its realization in REDUCE system, in: Proceedings of the International Symposium on Symbolic and Algebraic Computation, 1990, pp. 212–224.
[26] W. Research, The mathematical functions site, 1998, https://functions.wolfram.com. (Accessed 02 September 2022).
[27] M.A. Esmail, H. Fathallah, M.-S. Alouini, Outage probability analysis of FSO links over foggy channel, IEEE Photonics J. 9 (2) (2017) 1–12.
[28] A. Papoulis, S.U. Pillai, Probability, Random Variables, and Stochastic Processes, fourth ed., McGraw Hill, New York, 2002.
[29] T.Y. Elganimi, Studying the BER performance, power-and bandwidth-efficiency for FSO communication systems under various modulation schemes, in: 2013 IEEE Jordan Conference on Applied Electrical Engineering and Computing Technologies, AEECT, IEEE, 2013, pp. 1–6.
[30] M. Usman, H.-C. Yang, M.-S. Alouini, Practical switching-based hybrid FSO/RF transmission and its performance analysis, IEEE Photonics J. 6 (5) (2014) 1–13.
[31] H. Tapse, D.K. Borah, Hybrid optical/RF channels: Characterization and performance study using low density parity check codes, IEEE Trans. Commun. 57 (11) (2009) 3288–3297.
[32] T. Rakia, H.-C. Yang, M.-S. Alouini, F. Gebali, Outage analysis of practical FSO/RF hybrid system with adaptive combining, IEEE Commun. Lett. 19 (8) (2015) 1366–1369.
[33] K.O. Odeyemi, P.A. Owolawi, Selection combining hybrid FSO/RF systems over generalized induced-fading channels, Opt. Commun. 433 (2019) 159–167.
[34] N.D. Chatzidiamantis, G.K. Karagiannidis, E.E. Kriezis, M. Matthaiou, Diversity combining in hybrid RF/FSO systems with PSK modulation, in: 2011 IEEE International Conference on Communications, ICC, IEEE, 2011, pp. 1–6.
[35] Z. Ghassemlooy, M. Uysal, M.A. Khalighi, V. Ribeiro, F. Moll, S. Zvanovec, A. Belmonte, An overview of optical wireless communications, Opt. Wirel. Commun. (2016) 1–23.
[36] I.S. Ansari, S. Al-Ahmadi, F. Yilmaz, M.-S. Alouini, H. Yanikomeroglu, A new formula for the BER of binary modulations with dual-branch selection over generalized-K composite fading channels, IEEE Trans. Commun. 59 (10) (2011) 2654–2658.